Journal of Molecular Liquids 305 (2020) 112826

Contents lists available at ScienceDirect

Journal of Molecular Liquids

journal homepage: www.elsevier.com/locate/molliq

Characterization of the solvent specific evaporation from a fluoropolymer surface roughened by layered double oxide (LDO) particles

Ildikó Y. Tóth [a,*], László Janovák [b], Erzsébet S. Bogya [c], Ágota Deák [b], Imre Dékány [b], Amit Rawal [d], Ákos Kukovecz [a]

[a] University of Szeged, Interdisciplinary Excellence Centre, Department of Applied and Environmental Chemistry, H-6720, Rerrich Béla tér 1, Szeged, Hungary
[b] University of Szeged, Interdisciplinary Excellence Centre, Department of Physical Chemistry and Materials Science, H-6720, Rerrich Béla tér 1, Szeged, Hungary
[c] MTA-SZTE "Lendület" Porous Nanocomposites Research Group, Rerrich Bela sq. 1, Szeged H-6720, Hungary
[d] Indian Institute of Technology Delhi, Hauz Khas, New Delhi, India

ARTICLE INFO

Article history:
Received 25 October 2019
Received in revised form 25 February 2020
Accepted 1 March 2020
Available online 3 March 2020

Keywords:
Wetting
Evaporation
Hydrophobic
LDO/fluoropolymer composite
Model calculation
Qualitative analytics

ABSTRACT

Solid/ liquid interaction strongly depends, among other things, on the chemical and physical properties of fluids, therefore, there are unexploited analytical possibilities in investigating the surface wetting and evaporation behavior. Strongly hydrophobic rough surface thin films were prepared by spray-coating a fluoropolymer film with incorporated layered double oxide (LDO) microparticles. We studied the evaporation of ethanol–water mixtures from the low energy (8.4 ± 2.6 mJ/m^2) composite surfaces by simultaneous high-speed visible imaging, infrared imaging and weight loss monitoring. The wetting behavior changed from Cassie's wetting mode (pure water) to Wenzel's (pure ethanol) as a function of solvent composition. The vaporization process could be divided into three stages described by constant evaporate rates and the heat transfer coefficient between the studied layer and water is $K_T = 1768$ W/(m^{2}K). We have found strong correlations between parameters of the measured evaporation profiles and certain physical properties of the solvents. It is possible to estimate the viscosity, the boiling point, or the surface tension of a studied liquid merely from the total evaporation time. This novel solvent identification method can serve as a new application field for such low energy hybrid surfaces.

1. Introduction

Recent developments in nanotechnology have highlighted the importance of the classical topics of wetting, droplet spreading and evaporation [1–4]. These phenomena govern several key technological applications like oil recovery [5,6], efficient deposition of pesticides on plant leaves [5], controlled deposition of self-assembled surface coatings [7–10], micro-fluidics [5,11,12] and inject printing [5,13].

The evaporation of sessile droplets on solid surfaces can be categorized into three basic scenarios. The first case is the evaporation of simple solutions on plain surfaces. For this type two modes of evaporation can be distinguished: vaporization with decreasing contact radius at constant contact angle (CCA) or with decreasing contact angle at constant contact radius (CCR) [14,15]. The second case is the evaporation of simple fluids on micro and/or nano-structured surfaces. According to some opinion, a sessile droplet has two possible equilibrium wetting states on a rough surface. In the Cassie's state the droplet sits on the top of the protrusions of the surface, whereas in Wenzel's state the fluid wets the grooves between the protrusions [16]. Due to their different local minimum energy states, the transformation phenomenon from Cassies's mode to Wenzel's mode can occur, which is called wetting mode transition and reduces the contact angle drastically [1]. These rough surfaces are frequently superhydrophobic substrates, on which the droplet evaporation usually follows either the CCA, the CCR, or the mixed mode [17,18]. The third case is the evaporation of fluids containing dispersed nanoparticles from plain surfaces. The presence of colloidal particles in a solvent modifies the evaporation rate of the fluid [19]. After the vaporization of the liquid, solid particles remain on the surface, which can be used for surface decoration. In some case, the dried deposit is not uniform, which is caused by the enhanced evaporation at the wetting line. The so-called coffee-ring patterns develop during this phenomenon [20,21].

The evaporation rate of a droplet depends on several parameters, such as the chemical composition of solid surface and liquid, the temperature, the boiling point, the surface tension, *etc.* The evaporation takes place on the liquid/gas surface, therefore, the interface size is one of the dominant parameters. In a typical liquid/solid system the interface size is determined by the surface wettability. Four surfaces types can be distinguished on this basis: the superhydrophobic (contact angle >150°), hydrophobic (contact angle >90°), the hydrophilic (contact angle <90°) and the superhydrophilic (contact angle <5°) [15,22].

* Corresponding author at: I.Y. Tóth, H-6720, Rerrich Béla tér 1, Szeged, Hungary.
E-mail address: ildiko.toth@chem.u-szeged.hu (I.Y. Tóth).

https://doi.org/10.1016/j.molliq.2020.112826

Various techniques are available to modify the wettability of a surface. For example, UV and ozone treatment of carbon nanotube arrays yields a superhydrophilic surface, while annealing the same nanotubes in vacuum results in a superhydrophobic surface [22].

Layered double hydroxides (LDHs) are well-known synthetic clays. The layers are positively charged due to the divalent (Mg^{2+}, Ca^{2+}, Zn^{2+}) and trivalent cations (Al^{3+}, Fe^{3+}, Cr^{3+}) in their sheets. This charge is compensated by anions (OH^-, Cl^-, CO_3^{2-}, NO_3^-) between the sheets [23,24]. LDHs have very wide-ranging application possibilities: they can be used as adsorbents [25–27], coating materials [28], flame retardants [29], antacids [30], medicine stabilizers [30] and even as catalysts in several different reactions [26,30,31]. Furthermore, LDHs containing Zn^{2+} can serve as starting materials for the synthesis of ZnO-containing layered double oxides (LDOs). These calcined LDO microparticles with spherical shape and rough surface are photocatalytically active under UV-A illumination and they can be used for the synthesis of LDO/fluoropolymer hybrid layers with micro- and nano-sized dual-scale surface roughness [32]. They have systematically varied the loading of the hydrophilic LDO particles in hydrophobic LDO/fluoropolymer layers to tune the surface roughness and the wetting properties of the LDO/fluoropolymer films, and demonstrated that both superhydrophilic (at 100% LDO loading) and superhydrophobic (at ~85% LDO loading) rough films can be prepared by this method [32].

The evaporation of a sessile droplet can be studied by several experimental methods: transmission electron microscopy [33], environmental scanning electron microscopy [33,34], contact angle measurement [15,16,35–37], high speed camera recordings [38–40], thermal imaging [41], just to name a few. There are several parameters characteristic for the evaporation process [39,41], the most important ones being the evaporation time (from the surface or from the porous structure of porous materials), the contact angle (its initial value and its change in time), and the evaporation rate (weight loss as a function of time).

The main goal of the present work was to obtain a more detailed picture of the surface properties – namely, the wetting and vaporization properties – of the strongly hydrophobic LDO/fluoropolymer for different solvents. This knowledge can contribute to the development of the novel, evaporation based analytical method coined earlier by us as evaporation profile measurement [39]. The evaporation of different solvents from the surface of the low energy LDO/fluoropolymer hybrid layer was characterized by simultaneous weight monitoring, high-speed and infrared imaging. Furthermore, the experimentally determined evaporation parameters were analyzed statistically to assess the feasibility of using this hybrid material in potential analytical applications.

2. Materials and methods

2.1. Materials

$Zn(NO_3)_2 \cdot 6\ H_2O$ (99%, Fluka Chimika), $Mg(NO_3)_2 \cdot 6\ H_2O$ (98%, Sigma-Aldrich), $Al(NO_3)_3\ 9\ H_2O$ (99.7%, Molar), urea (98%, Sigma-Aldrich), 1H,1H, 2H, 2H-perfluorodecyl acrylate (Aldrich), and 2,2-dimethoxy-2-phenylacetophenone (Aldrich) were used for LDO/fluoropolymer thin film preparation. Milli-Q water (0.059 μS/cm) was used for the experiments. Ethanol (EtOH) and toluene were analytical grade products purchased from Molar. The composition of the ethanol-water mixtures was expressed in weight percent (wt%).

2.2. Preparation of the LDO/fluoropolymer composite thin layer

Spherical LDH microparticles with rough surface were prepared by co-precipitation from the solutions of zinc nitrate, magnesium nitrate, aluminum nitrate and urea precursors. The molar ratio of Zn/Mg was 0.125 and the molar ratio of (Zn+Mg)/Al were 2.00. The mixture was aged at 98 °C for 7 days. After the aging process, the formed precipitate was dried at 60 °C overnight. The spherical LDO particles were prepared by the calcination of ZnMgAl-LDH powder at 600 °C for 2 h. The prepared LDO particles measured ~25 μm in diameter. Their rough, structured surface was created by the radial arrangement of their conventional hexagonal lamellae [32,42]. The low-energy poly(1H,1H, 2H, 2H-perfluorodecyl acrylate) [p(PFDAc)] fluoropolymer was synthetized from PFDAc monomer and 2,2-dimethoxy-2-phenylacetophenone photo initiator by free-radial UV polymerization method (Q81 type lamp, Heraeus Gmbh, power: 70 W, $\lambda_{max} = 265$ nm, 30 min) [32,43]. The prepared p(PFDAc) was dissolved in toluene, in which the fluoropolymer content was 10 wt%. The LDO loaded toluene-based suspension was prepared (with 80 wt% LDO and 20 wt% fluoropolymer content for the dried material) and it was sprayed on 5 cm × 5 cm glass substrate from 15 cm distance using an R180 type Airbrush spray gun with 3 bar operating pressure. The detailed characterization of the prepared LDO/fluoropolymer composite was reported earlier [32].

2.3. Contact angle measurements

The advancing (Θ_{adv}) and receding (Θ_{rec}) contact angles were determined with the drop-build-up technique using distilled water as test liquid. The measurements were performed under atmospheric pressure and constant humidity, applying an EasyDrop drop shape analysis system (Krüss GmbH, Hamburg, Germany) equipped with DSA100 software, a Peltier temperature chamber and a steel syringe needle of 0.5 mm diameter and using distilled water as a test liquid. According to the theory of Chibowski et al. [44] the obtained Θ_{adv} and receding Θ_{rec} – *i.e.* the contact angle hysteresis (CAH) – are also suitable for the estimation of the total apparent surface free energy (γ_s^{tot}) of the layer, knowing the surface tension of the probe liquid, (γ_l, 72.1 mN/m in the case of distilled water at 25 °C) and its contact angle hysteresis, which is defined as the difference between the Θ_a and Θ_r [44]:

$$\gamma_s^{tot} = \left(\frac{\gamma_1 (1 + \cos\theta_a)^2}{(2 + \cos\theta_r + \cos\theta_a)} \right) \quad (1)$$

The general feature of the apparent surface free energy as a function of CAH relationship is the decrease in energy with increasing hysteresis. The relative decrease of the apparent surface free energy is strongly sensitive to the advancing contact angle value. However, in the case of rough surfaces advancing contact angle by itself is not enough for solid surface free energy determination, because often advancing contact angle measured on left and right hand side of the droplet is significantly different. Therefore, the total surface free energy of a solid can be evaluated from three measurable parameters, *i.e.* probe liquid surface tension and its advancing and receding contact angles measured on the investigated solid surface.

To follow the evaporation process, the static contact angle of 5 μL ethanol-water mixture droplets on LDO/fluoropolymer film was measured with a Vision Research Miro 110LC fast camera with Nikon 105 mm macro lens at 24 frame/s recording speed, at 1280 × 720 resolution and at 4000 μs exposure time. The droplets were instilled with an Eppendorf Xplorer electronic pipette on the LDO/fluoropolymer layer. The measurements were performed under atmospheric pressure, at room temperature (25.4 °C) and at 55% relative humidity. The images extracted from the video were further analyzed with the ImageJ program. The size and the shape of the liquid droplets changed continuously during the evaporation. To characterize this process, the variation of contact angle and diameter characteristic for the interface between surface and liquid were determined by ImageJ software using the pictures exported from the recorded video at selected moments.

2.4. Thermal imaging and mass measurements

The evaporation of different solvents (5 μL water, ethanol and their mixtures) from the LDO/fluoropolymer film was studied. The films

were kept at a constant 50 ± 1 °C by a purpose-built, Peltier cell based temperature controller. The sample holder was placed on a Sartorius Cubis MSU225S-000-DU microbalance with 0.01 mg readability. The balance was linked to a data acquisition computer and the experimental data were collected by StartoCollect software during the evaporation. A FLIR A655sc infrared (IR) camera was fixed vertically above the LDO/ fluoropolymer film, looking directly downwards in a direction normal to the top surface of the film. The schematics of the equipment were reported previously [41]. The liquid droplets (at room temperature) were instilled with the same Eppendorf Xplorer electronic pipette on the surface of the film and the temperature and weight variation were simultaneously recorded during the evaporation process.

The FLIR A655sc IR camera has a thermal sensitivity of 30 mK, an accuracy of ±2 °C for temperatures up to 650 °C at 640 × 480 resolution. Its uncooled micro bolometer detector works in the 7.5–14.0 μm spectral range. During the experiments, the infrared camera was equipped with a 2.9 × (50 μm) IR close-up lens, with 32 × 24 mm field of view and 50 μm spatial resolution. Sessile droplet evaporation movies were recorded by FLIR Research IR software at maximum resolution with 25 Hz frame rate. The emissivity of LDO/polymer film ($\varepsilon_{film} = 0.99$) was determined by calibration at the initial film temperature (50 °C) with a FLIR tape ($\varepsilon_{tape} = 0.95$). During the surface evaporation of the liquid droplets, the temperature was calculated by using the emissivity of the liquids ($\varepsilon_{liquid} = 0.95$); after surface evaporation, the emissivity of the wetted film was calculated as the average between ε_{film} and ε_{liquid} [41]. The hybrid films were kept at 50 ± 1 °C, the atmospheric temperature and the initial temperature of the liquid droplets were 21.1 °C and the relative humidity was 51% during the experiments. The videos and their extracted images were analyzed by FLIR Research IR and ImageJ software.

3. Results and discussion

We used LDO particles roughened fluoropolymer thin film as model surface because in our previous paper it was reported that the composite films with increasing LDO content have porous multilayer structure and the porosity of the films is varied between 17.5 and 58.1% [32]. The measured thickness values of the layers were varied between 64 and 201 μm and increased with the increase in LDO content. Therefore, these composite layers with porous structure and roughened surfaces, but non- water wetting characteristic seemed like an ideal choice for the characterization of solvent specific evaporation. In case of porous solid materials, the evaporation of a liquid drop is a complex phenomenon. Several separable steps take place consecutive and parallel, *e.g.* drop impact on the surface, spreading, wetting, capillary imbibition, evaporation from the surface and pores [39]. The partial or complete wetting process of a droplet on thick porous layers can be divided into more stages: first the imbibition front in the porous layer moves slightly ahead of the spreading droplet on the layer, later it expands further while the base of the sessile drop starts to shrink, and finally the imbibition front disappears at the end of the drying process [45–47]. The effect of the substrate's thermal properties is very significant on the evaporation rate of a sessile droplet and the heat transfer from the solid layer is particularly pronounced on a heated substrate [38,48].

The evaporation of EtOH-water mixtures (with 0%, 30% 70% and 100% EtOH content) from the surface of LDO/fluoropolymer was monitored by three different experimental methods. In the first part of the discussion, the results of these methods are discussed separately. The contact angles as a function of time are determined from the videos recorded by high speed visual imaging. The wetting mode characteristic for the different solvents can be specified from these data. The sessile droplet on the film surface and the liquid in the porous system of the solid can be distinguished from each other by evaluating the videos recorded by the infrared camera [39,41]. In this case, the time dependent spot area and temperature carry the information. Finally, the total evaporation time and the evaporation rate can be determined from the mass measurements. In the second part of the discussion, the uncovered relationships were analyzed between the selected characteristic experimental parameters and the physical properties of the mixtures, in order to assess the analytical possibilities of the system.

3.1. Contact angle measurements

The solid free surface energy of the LDO/ fluoropolymer composite can be estimated from dynamic (Θ_a and Θ_r) contact angles measurement using Chibowski theory [44]. Fig. 1a indicates that increasing the volume of the water drop leads to reduction of the Θ_a from $\Theta_{11.6\mu l} = 139.4 \pm 1.63°$ to $\Theta_{44.66\mu l} = 133.8 \pm 2.1°$. The Θ_r were gradually decreasing as the volume of the drop was decreasing and the final value was much lower (102.3 ± 1.45°) than the initial Θ_a (=139.4 ± 1.63°). The γ_s^{tot} of the LDO/fluoropolymer layers were 8.4 ± 2.6 mN/m, which are characteristic for hydrophobic surfaces with adequate surface roughness, and are significantly lower than those of low energy, flat Teflon-like coatings (γ = ~20–22 mN/m), matching the available published data well [32].

A high speed camera was used to monitor the evaporation of different solvents from the surface of LDO/fluoropolymer layers from a horizontal perspective. The static contact angles (Θ) as a function of time are shown in Fig. 1b. The time of evaporation from the surface ($t_{s(\Theta)}$) increased from ~80 s to ~850 s with decreasing amount of ethanol in the solvent mixtures. This is in a good agreement with the well-known experience that ethanol with lower surface tension (γ = 21.82 mN/m at 25 °C) evaporates faster than water with higher surface tension (γ = 72.1 mN/m at 25 °C). For the systematic evaluation of the droplet's evaporation rate, the surface tension of the ethanol/ water mixture can be arbitrarily tuned by the ratio of these two miscible solvents. The contact angles decreased as a function of time for all studied solvent mixtures, however, their time dependence was characteristic for the chemical composition of the mixture. The initial contact angles decreased systematically with increasing ethanol content, *i.e.* the contact angles at $t = 0$ s (Θ_{in}) were 129°, 119°, 114° and 110° in case of 0%, 30%, 70% and 100% ethanol content, respectively.

To facilitate the comparison of the vaporization of solvents with very different evaporation times, let us define the relative time $t_{rel} = t/t_s$ where t_s is the time of evaporation from the surface. The relative changes of contact angles and contact diameters were plotted as a function of relative time in Fig. 1c and d.

In the first part of the vaporization (approximately until the half of the surface evaporation time, *i.e.* up to $t/t_{s(\Theta)} = 0.5$), the contact angles characteristic for the droplet of water and the 30% ethanol content mixture are only slightly reduced, whereas these samples exhibit significant contact diameter decreases. This behavior (CCA evaporation mode) is characteristic for non-wetting solutions, such as water evaporation from hydrophobic surfaces [15,49]. The interaction between these liquids and the rough LDO/fluoropolymer layer can be described by the Cassie-Baxter wetting where air pockets remain trapped under the solid-liquid interface [15,16]. On the other hand, the contact angle decreases very strongly and the contact diameter increases continuously during the evaporation of the ethanol droplet. In case of rough hydrophobic surfaces this phenomenon is typical for the wetting mode transition from Cassie-Baxter wetting to Wenzel wetting [16,49]. The LDO/ fluoropolymer layer is wetted much better by ethanol than by water, and the evaporation is much faster in case of ethanol, too. The vaporization behavior of the 70% ethanol content mixture droplet is somewhere between the evaporation of pure water and pure ethanol, namely, up to $t/t_{s(\Theta)} = 0.5$ the contact diameter is almost constant (CCR evaporation mode) and the contact angle decreases at a medium rate.

3.2. Measurements by infrared camera

Infrared imaging was used to monitor the vaporization of the solvent mixtures from the hydrophobic surface of the LDO/fluoropolymer layer

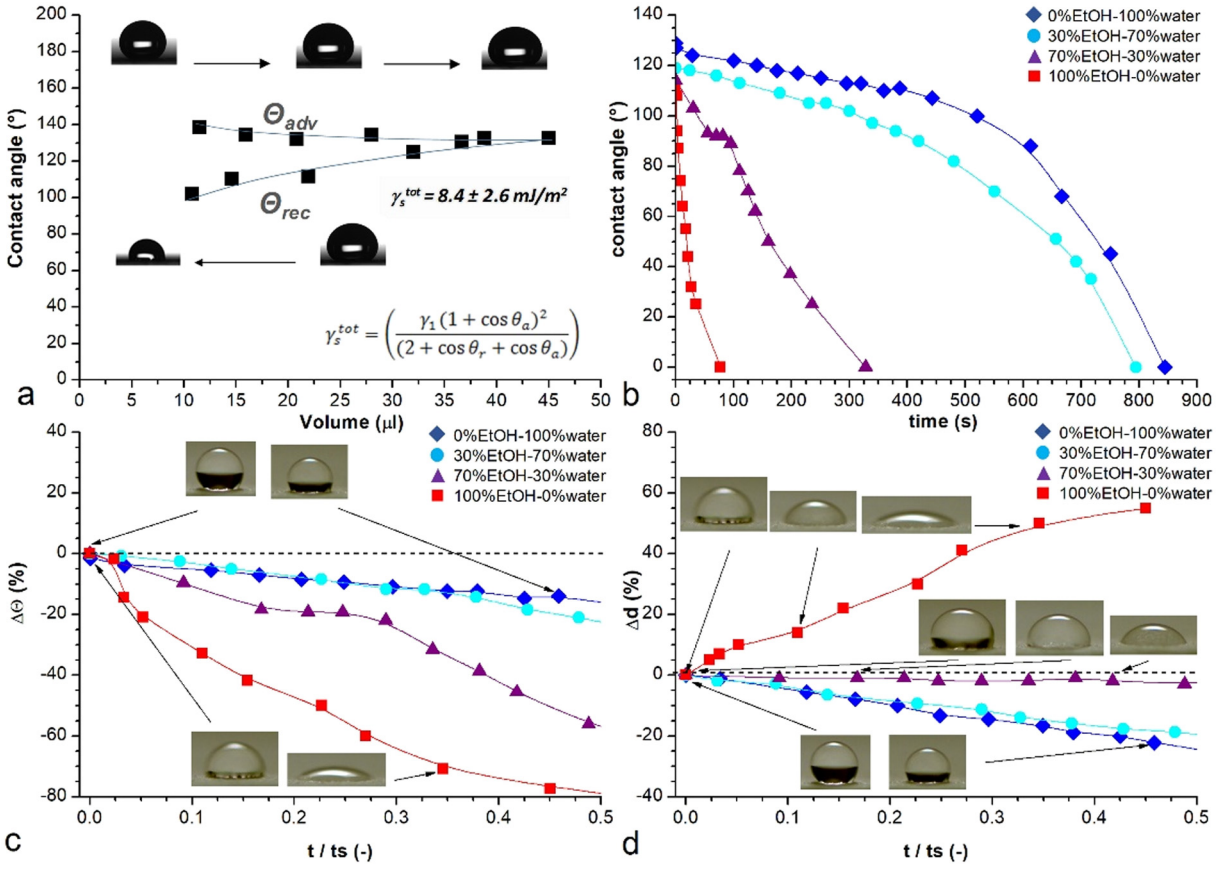

Fig. 1. Contact angle measurements. a) Evolution of advancing (Θ_a) and receding (Θ_r) water contact angles on LDO/fluoropolymer layer. The evaporation of different solvents from the hybrid layer characterized by high speed camera: b) measured static contact angles (Θ) as a function of time; c) static contact angles and d) spot diameters shown on a relative time scale, where $t_{s(\Theta)}$ is the time of evaporation from the surface. (The representative pictures were exported from the videos. The experiments were carried out under atmospheric pressure, at room temperature, at constant humidity and the droplet volume was 5 μL. The lines serve as guides for the eye. ($Error_\Theta$: ±3°; $Error_d$: ±2 pixel.)

from a vertical perspective. The videos were evaluated at selected representative moments. In Fig. 2 the determined spot area and average temperature of the drop (S_d, T_d) and of the wetted region (S_w, T_w) are plotted as a function of relative time. The evaluated data characteristic for the different liquids is reported in Table 1.

The initial area of the droplets ($S_{d(t0)}$) was almost the same for 0%, 30% and 70% ethanol content solvents and its value was more than one and a half times for ethanol (see Table 1). In the range of 0.5–1.0 relative time, the S_d values were decreasing continuously for all studied liquids, however, there were significant differences in the initial range. For water and 30% ethanol content mixture the S_d decreased definitely, while for 70% ethanol content the S_d was approximately constant up to $t_{rel} = 0.5$, over and above the area of the ethanol drop increased significantly during this period. These observations match the contact angle based findings discussed above well. At the end of the surface evaporation ($t_{s(IR)}$): $S_d = 0$ and $t_{rel} = 1$.

The initial areas of the wetted region ($S_{w(t0)}$) are almost equal to the $S_{d(t0)}$ for all studied solvents, the difference being no >1 mm^2 (~15%) in any case. At the same time, there are significant differences in their time dependence (see Fig. 2). During the evaporation of pure water, the S_w value decreases parallel with S_d. At the moment of the total surface evaporation, the wetted area is only $S_{w(ts)} = 1.19\ mm^2$ and this minimal remaining water, which can be found in the porous system of LDO/polymer layer, evaporates in a very short relative time. By contrast, the temporal evolution of the S_w is completely different during the vaporization of ethanol. The wetted area increases continuously: at $t_{rel} = 1$ $S_{w(ts)}$ equals 18.04 mm^2. During the evaporation of ethanol from the porous system, the wetted area keeps increasing and reaches its maximum at $t_{rel} = 9.7$, where $S_{w(max)} = 27.22\ mm^2$, more than three times its initial value. In the last phase of the evaporation, the area of the wetted region decreases rapidly down to $S_w = 0\ mm^2$ at the total evaporation time ($t_{t(IR)}$). This characteristic difference observed for water and ethanol can be explained by the different wetting properties of these solvents, as described previously.

The surface evaporation time $t_{s(IR)}$ values are 756 s, 324 s, 104 s and 3.8 s, and the total evaporation time $t_{t(IR)}$ values are 825 s, 423 s, 199 s and 61 s for the mixtures with 0%, 30%, 70% and 100% ethanol content, respectively. The behavior of data is similar to the observed trend obtained for the time of evaporation from the surface ($t_{s(\Theta)}$) at the contact angles measurements, but the magnitudes are different. The times required for evaporation from the surface are systematically smaller in case of the infrared measurements, which can be plausibly explained by the higher temperature (50 °C) during the experiment.

To improve the infrared contrast, solvents were kept at room temperature before the experiments. Therefore, there was a temperature difference between the initial 5 μL drops and the LDO/fluoropolymer layer kept at 50 °C. The temperature of the liquid and the solid is changed continuously during the experiment because of the initial difference, the heating of the LDO/fluoropolymer layer, the endotherm evaporation process, *etc.* The temperature change profile is characteristic for each measured solvent. The variations of average temperature for the drop (T_d) and wetted region (T_w) were plotted as a function of time in Fig. 2. The temperature variation along the diameter of the solid surface for different solvents at t_0 and t_s is represented in Fig. 3. While the T_d and T_w temperatures increase continuously for all ethanol-containing mixtures, there is a longer constant temperature period (almost 6 min) in the case of the evaporation of pure water from the studied surface.

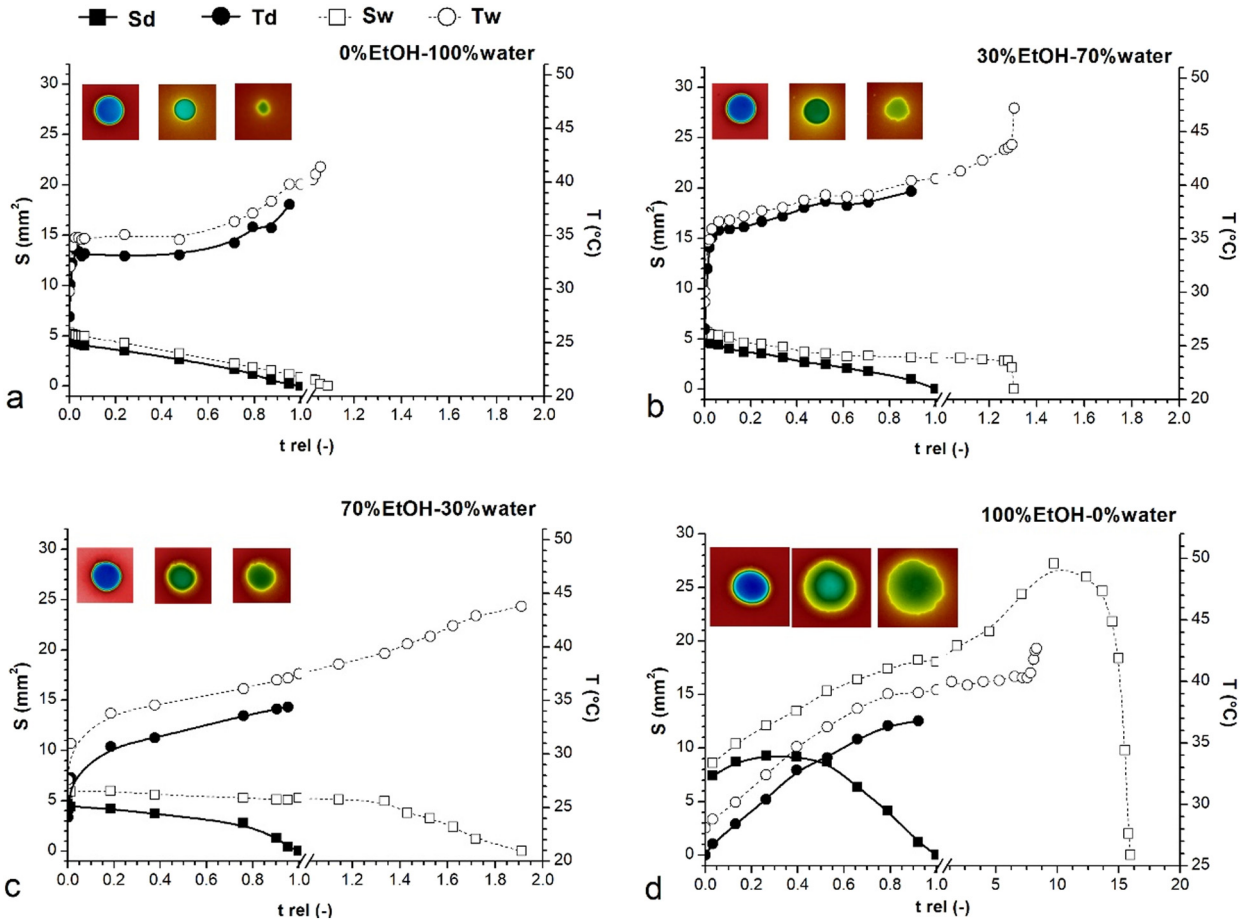

Fig. 2. The variation of the area (S) and average temperature (T) of the droplet on surface ($_d$) and of the wetted region ($_w$) as a function of relative time ($t/t_{s(IR)}$) during the evaporation of different ethanol-water mixtures (with a) 0%, b) 30%, c) 70% and d) 100% EtOH content) from LDO/fluoropolymer layer. The images in the upper left corners (exported *pro rata* from the IR video) correspond to t_0, a representative intermediate time t, and t_s. The temperature of the solid was set to 50 °C. The droplets were 5 μL. (Error T: ±1 °C; Error $_S$: ±0.5mm^2.)

3.3. Weight loss measurements

Droplets of different solvents were placed on the LDO/fluoropolymer layer and their measured weight variations are shown in Fig. 4. The shapes of the weight variation curves are characteristic for the evaporating solvents. These peaks can be characterized by their maximum value (*i.e.*, m_{max}), full width at half maximum (FWHM), full width at base (at m = 0 mg, i.e., total evaporation time, $t_{t(m)}$) and the slope of the decline (dm/dt). These parameters are summarized in Table 2.

Within the error of the measurements, the average maximum weight data (m_{max}) agree well with the theoretical values of the 5 μL drops' initial masses at room temperature, namely 4.99 mg, 4.77 mg, 4.34 mg and 3.95 mg in case of 0%, 30%, 70% and 100% ethanol content, respectively. The total time of evaporation ($t_{t(m)}$) increases from ~50 s to ~790 s with decreasing amount of ethanol in the solvent mixtures (see Table 2), and these data correlate well with the total evaporation time determined from the IR measurements ($t_{t(IR)}$, see Table 1).

Table 1
Data extracted from infrared videos characteristic for the evaporation of different solvents from LDO/fluoropolymer layer. $S_{d(t0)}$ is the initial area of the drops, $S_{w(ts)}$ is the area of the wetted region at the end of the surface evaporation (t_s) and t_t is the total evaporation time. The temperature of the solid was set to 50 °C. The droplets were 5 μL.

Solvent mixture	$S_{d(t0)}$ (mm^2)	$S_{w(ts)}$ (mm^2)	$t_{s(IR)}$ (s)	$t_{t(IR)}$ (s)
0%EtOH-100%water	4.69	1.19	756	825
30%EtOH-70%water	4.95	3.11	324	423
70%EtOH-30%water	4.68	5.26	104	199
100%EtOH-0%water	7.41	18.04	3.8	61

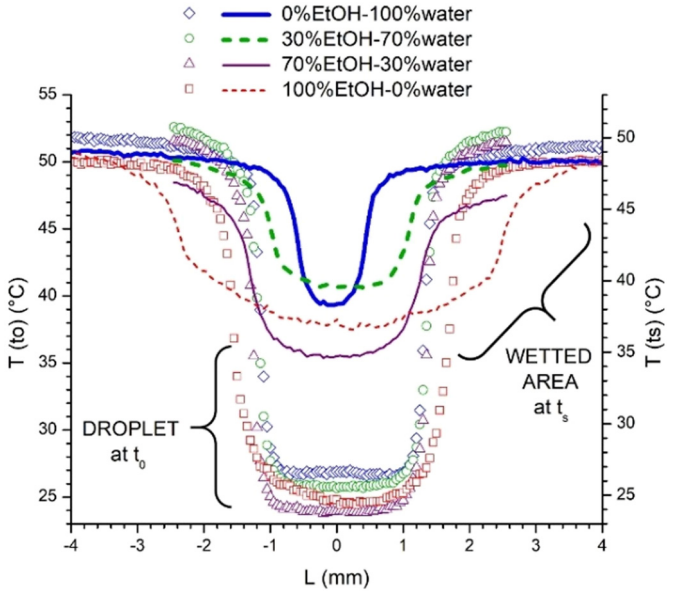

Fig. 3. Temperature variation along the diameter of the hydrophobic LDO/fluoropolymer for different liquids at initial moments of evaporation (t_0) and at the total surface evaporation (t_s). The temperature of the solid was set to 50 °C, the liquids were kept at room temperature. The droplets were 5 μL. (Error$_T$: ±1C°).

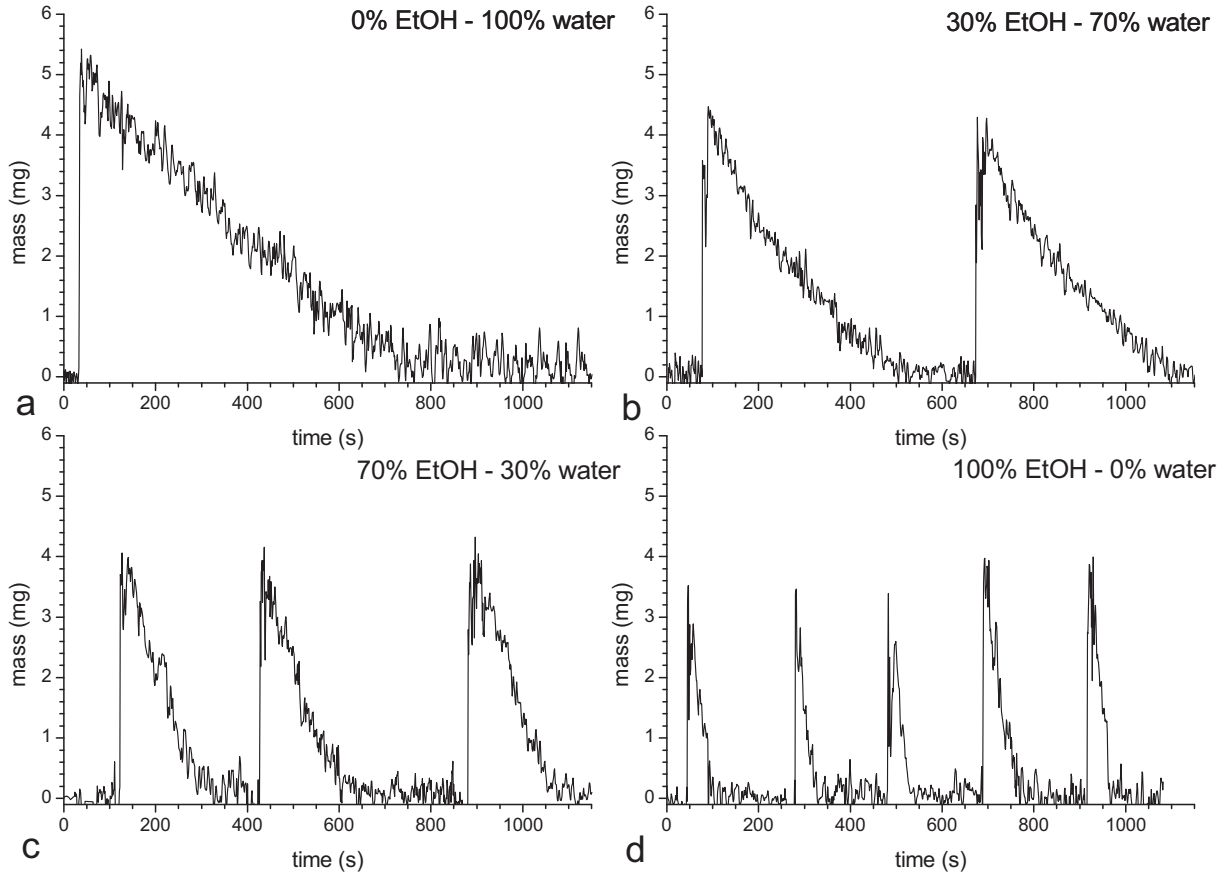

Fig. 4. Weight variation of the LDO/fluoropolymer layer as a function of time during the evaporation of different solvents. The temperature of the solid was set to 50 °C. The droplets were 5 μL.

At the end of the surface evaporation ($t_{s(IR)}$), well defined quantities of the solvent mixtures (m_s) remain in the pore system of the LDO/fluoropolymer layer. These quantities were 0.11 mg ± 0.04 mg, 0.67 mg ± 0.03 mg, 1.64 mg ± 0.12 mg and 3.18 mg ± 0.15 mg for 0%, 30%, 70% and 100% ethanol content solvent mixtures. To put these into perspective, these values correspond to 2%, 14%, 38% and 81% of the original liquid amount remaining in the porous system after the surface evaporation, respectively.

The slopes of weight loss (*dm/dt*) (*i.e.*, the rate of evaporation) for the different solvents were determined by fitting as reported in Table 2. These values are characteristic for the whole evaporation process and specific for the ethanol content of the solvents. The fitted *dm/dt* values correlate well with the calculated – $m_{max}/t_{t(m)}$ values. Hence the slope of weight loss, the total evaporation time and the density of the solvent (which defines the initial mass) are all related to each other.

In case of a porous solid material, the weight loss of the liquid measured during the vaporization can be explained i) by the evaporation of the sessile droplet on the solid (its rate depends for example on the shape of the drop, so it is obviously different for a drop with contact angle (θ) >90°or <90° [15,50,51] shown in Fig. S1) and ii) by the evaporation from the porous system (condensed or adsorbed liquid). The evaporation phenomenon can be divided into different stages, and typically, different dominant process can be assigned to each stage. Thus, in theory, evaporation of a liquid from LDO/fluoropolymer layer can be divided into three stages: in the I stage the dominant process is the evaporation of the sessile droplet with θ >90°; in the II stage the dominant process is the evaporation of the sessile droplet with θ <90° (until t_s) and in the III stage the dominant process is the evaporation of the liquid from the porous system (until t_t). These stages for the evaporation of ethanol-water mixtures from LDO/fluoropolymer layer are shown in Fig. 5 and in the Supplementary Table S1. The evaporation rate (dm/dt) for the divided vaporization stages were determined by linear fitting as reported in Table 3. Based on the results we can conclude, that i) the evaporation rate for the divided stages of the vaporization is constant with a good approximation, ii) the evaporation rate decreases systematically in the successive stages, and iii) the evaporation rate increases with the increasing ethanol content examining a selected stage.

Approximate analytical expression of the evaporation rate can be described by different mathematical models for the vaporization of sessile droplets with θ < 90° [21,41,52–54]. Since the constitution of the evaporating ethanol-water mixtures changes during the evaporation and the LDO/fluoropolymer layer shows a slight instability against

Table 2
Experimentally determined data characteristic for weight losses of the different solvent evaporations from LDO/fluoropolymer layer; $t_{t(m)}$ is the total evaporation time. The temperature of the solid was set to 50 °C. The droplets were 5 μL.

Solvent mixture	m_{max} (mg)	$t_{t(m)}$ (s)	FWHM (s)	dm/dt (mg/s)
0%EtOH-100%water	5.03 ± 0.04	792.1 ± 16.9	323.1 ± 21.8	−0.0067 ± 0.0002
30%EtOH-70%water	4.47 ± 0.22	428.7 ± 5.9	154.5 ± 10.5	−0.0092 ± 0.0005
70%EtOH-30%water	4.27 ± 0.21	182.8 ± 10.5	90.3 ± 8.8	−0.0211 ± 0.0005
100%EtOH-0%water	3.81 ± 0.72	49.8 ± 1.7	27.0 ± 4.3	−0.0678 ± 0.0108

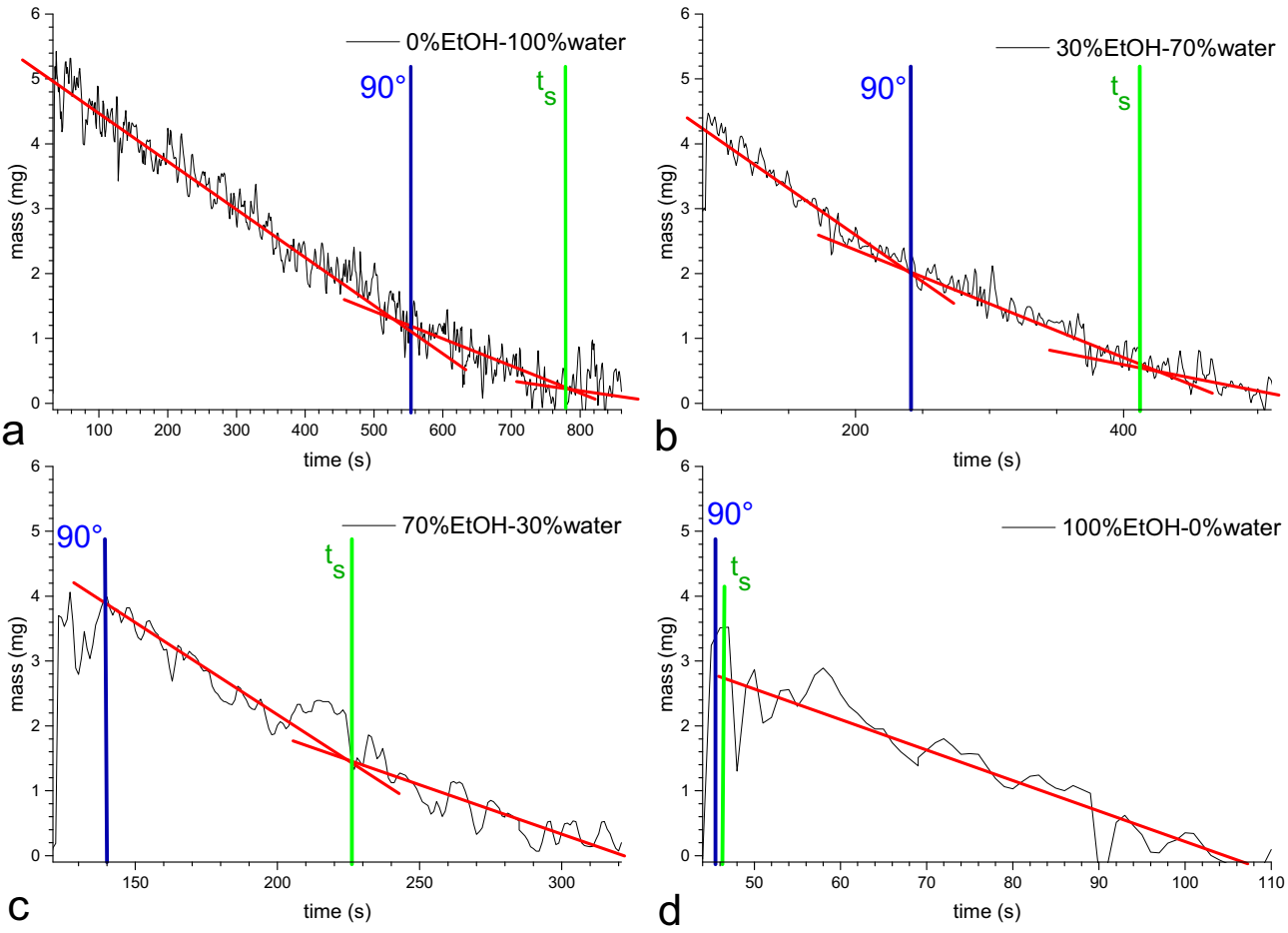

Fig. 5. Different stages for the evaporation of the ethanol-water mixtures from LDO/fluoropolymer layer. (t_s is the time of evaporation from the surface.) (The temperature of the solid was set to 50 °C. The droplets were 5 μL.)

pure ethanol, in this study only the evaporation rate of the pure water droplet with θ <90° will be discussed in detail.

Hu and Larson [52] investigated the evaporation of a sessile water droplet from glass with pinned contact line described as a quasi-steady-state process. They conclude, that i) the net evaporation rate remains almost constant, ii) the evaporation flux becomes more strongly singular at the edge with the decreasing θ, and iii) the contact line starts to reduce only at θ ~2–4°. For θ <90° their model for the evaporation rate (dm/dt) is the following:

$$\frac{dm}{dt} = -\pi RD(1-H)c_v(1.27\theta + 1.30) \quad (2)$$

In Eq. (2) R is the contact line radius, D is the water vapor diffusivity, H is the relative humidity, c_v is the saturated water vapor concentration. Using this model, the evaporation rate values are constantly decreasing (from $dm/dt_{t=540s} = -0.0019$ mg/s to $dm/dt_{t=660s} = -0.0011$ mg/s) for the II stage of the water evaporation from LDO/fluoropolymer layer. These values are very far from those obtained experimentally, however, our system differs from Hu and Larson's system at several points: i) the solid is porous, ii) the liquid's temperature is continuously changing during the measurement, and iii) the contact line is not pinned during the evaporation.

Bogya et al. [41] build a model for the simulation of the evaporation of sessile water droplet (θ < 90°) from heated porous carbon nanotube films. The corresponding parameters were estimated for the actual temperature of the drop (T [K]). The full adaptation of this model for the LDO/fluoropolymer layer can be found in the Supplementary file (Eqs. (S1-S12)). The evaporation rate ($Q_m(T)$) and the energy balance equation are given by the following formulas:

$$Q_m(T) = D'_{wa}(T)\frac{S}{r_e}(c(T)-c_m) \quad (3)$$

Table 3
The evaporation rate (dm/dt) for the divided vaporization stages determined by linear fitting on the weight variation of the LDO/fluoropolymer layer as a function of time during the evaporation of different solvents. (The temperature of the solid was set to 50 °C. The droplets were 5 μL.)

Solvent mixture	I stage (from sessile droplet)	II stage (from sessile droplet)	III stage (from porous system)	Full range
	dm/dt (mg/s)	dm/dt (mg/s)	dm/dt (mg/s)	dm/dt (mg/s)
0%EtOH-100%water	−0.00708	−0.00502	−0.00082	−0.0067
30%EtOH-70%water	−0.01542	−0.00869	−0.00542	−0.0092
70%EtOH-30%water	–	−0.02785	−0.01481	−0.0211
100%EtOH-0%water	–	–	−0.05036	−0.0678

$$\frac{dT}{dt} = -\frac{K_T S_d (T - T_S)}{\rho(T) c_p(T) V} - \frac{\Delta H_V(T) Q_m(T)}{\rho(T) c_p(T) V} - \frac{K_{T,e} S (T - T_e)}{\rho(T) c_p(T) V} \quad (4)$$

In Eqs. (3) and (4) $D'_{wa}(T)$ is the diffusion coefficient of water in air [m^2/s], S is the surface area of drop [m^2], r_e is the equivalent diameter (of drop) [m], c(T) and c_m are the water vapor concentrations at the droplet-air interface and at the bulk air [kg/m^3]. In Eq. (4). T_S is the temperature of the solid support at the drop-solid contact area [K], T_e is the temperature of the surrounding air [K], K_T is the heat transfer coefficient between the solid support and the water droplet [$W/(m^2K)$], $K_{T,e}$ is the heat transfer coefficient between the water and the surrounding air [$W/(m^2K)$], S_d is the drop-solid contact area [m^2], $\rho(T)$ is the water density [kg/m^3], c_p is the specific heat of the water [kJ/(kgK)], ΔH_V is the evaporation heat of water [kJ/(kg)]. See the Supplementary for details (Eqs. (S1-S12).

The LDO/fluoropolymer layer has non- water wetting characteristic. The experimentally determined amount of the water in the porous layer is ~2% at the end of the sessile droplet's evaporation (t_s), thus, the diffusion flux of water to the solid phase was set to zero in the modelling of the vaporization. Using this model, the evaporation rate is −0.0038 mg/s for the II stage of the water evaporation from LDO/fluoropolymer layer, which slightly underestimates the experimental value, however, it is almost constant throughout the studied range (± 6%). The calculated heat transfer coefficient between the LDO/fluoropolymer film and the water droplet is $K_T = 1768$ $W/(m^2K)$.

3.4. Analysis of the characteristic experimental parameters – analytical possibilities

Evaporation characteristics appear to be noticeably specific for the chemical composition of the fluid and solid phase, as previously described. In order to demonstrate this phenomenon, some representative parameters determined from the experiments (*i.e.*, t_t, t_s, FWHM, dm/dt, $\Theta_{(t0)}$, $S_{d(t0)}$, $S_{w(ts)}$) were plotted as a function of the initial ethanol content in the liquid phase in Fig. 6. The presented changes are systematic: the values of t_t, t_s, FWHM, dm/dt, and $\Theta_{(t0)}$ decrease continuously, whereas $S_{d(t0)}$ and $S_{w(ts)}$ increase with the increasing ethanol content. The plotted points can be fitted mathematically by the $y = A \cdot e^{B \cdot x} + C$ expression. Note that this fitting formula does not support any direct physico-chemical interpretations. Fitted values of A, B, C, and the goodness of the fitting (R^2) are summarized in Table 4 for selected evaporation properties. The values of R^2 are above 0.978 for all studied cases, which confirms that it is valid to extract quantitative information from fitted values for an unknown ethanol-water mixture. Namely, the initial ethanol content can be determined by measuring the representative parameters calculated from the experiment performed using the unknown solution and by using the equations of the fitted curves as calibration curves. This method is likely to be applicable for other binary solvent mixtures as well.

It is intriguing to uncover relationships between the experimentally determined data and the physical properties of the studied solvents: the density (ρ), surface tension (γ), melting point ($T_{melting}$), boiling point ($T_{boiling}$), viscosity (η), dipole moment (p), and molecular mass (M) of the solvents were collected from widely accepted reference sources. For the studied liquids, the characteristic measured data (t_t, FWHM, dm/dt, t_s, $S_{d(t0)}$,$S_{w(ts)}$) and the physical properties of the solvents (ρ, γ. $T_{melting}$, $T_{boiling}$, η, p, M) are summarized in the Supplementary Table S2.

The matrix of Pearson correlation coefficients (PCC) was used to analyze this dataset. The relevant part of the PCC matrix can be found in Table 5, and all calculated Pearson correlation coefficients are reported in the Supplementary Table S3. The correlation between two chosen parameters is positive when the values increase together, and negative when one value decreases as the other increases. The absolute magnitude of coefficient is proportional to the strength of correlation. The characteristic ranges of PCC values are not unambiguously agreed on in the literature [55,56]. The ranges used in the present study are the following: 0.00 to 0.30 indicates negligible correlation, 0.30 to 0.50 is low correlation, 0.50 to 0.70 signifies moderate correlation (highlighted in green in Table 5), 0.70 to 0.90 means high correlation (highlighted in light blue) and 0.90 to 1.00 signals very high correlation (highlighted in dark blue).

It is essential to focus on the correlations between one measured value and one chosen physical property to uncover the relationships between experimentally determined data and the properties of solvents as defined by their physical properties. These PCC data can be found in the upper right quarter of Supplementary Table S3 and they are listed in Table 5 as the relevant part of PCC matrix.

There are very high correlations (|PCC| > 0.9) in about half of the cases, and high correlations for almost all other states as well (0.9 > |PCC| > 0.7). Data in Table 5 reveals that the t_t, t_s, FWHM, and $\Theta_{(t0)}$ parameters carry most of the information. For example, let us realize that it is possible to estimate the viscosity (PCC = −0.98), the boiling point (PCC = 0.96), or the surface tension (PCC = 0.95) of a studied liquid merely from the measured t_t value! Relationships presented in Table 5 allow us to estimate the physical parameters of the liquid, and thus obtain qualitative information for an unknown solvent based on the experimental results determined by our method.

4. Conclusions

The LDO/fluoropolymer composite layer with porous structure and roughened surfaces, but non- water wetting characteristic was our choice for the characterization of solvent specific evaporation. The

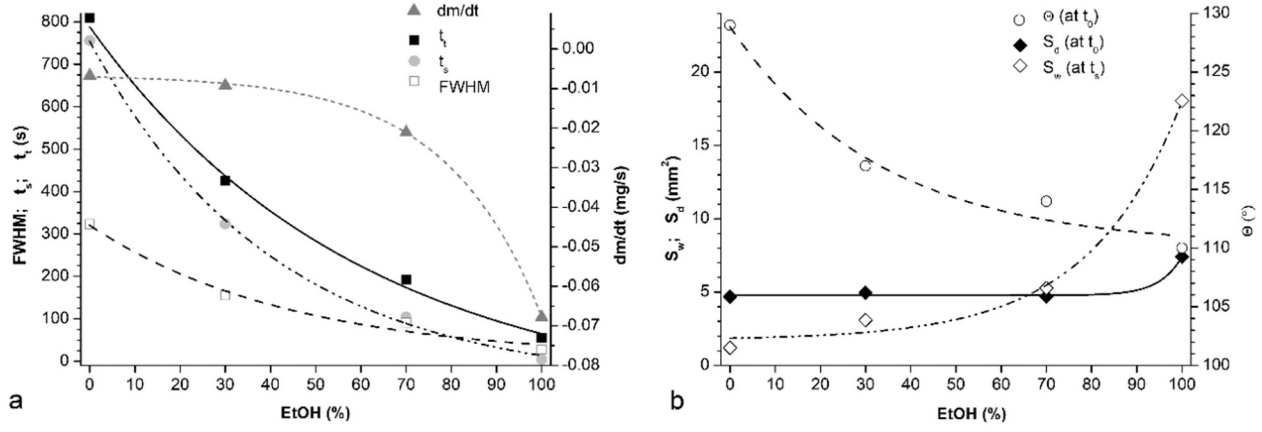

Fig. 6. The experimentally determined characteristic parameters of evaporation from LDO/fluoropolymer film plotted as a function of the initial ethanol content in the ethanol-water mixture. The points were fitted by $\boldsymbol{y = A \cdot e^{B \cdot x} + C}$. (This fitting formula does not support any direct physico-chemical interpretations.) The droplets were 5 μL.

Table 4
Fitted parameters of $y = A \cdot e^{B \cdot x} + C$ curves corresponding to experimentally determined evaporation parameters plotted as functions of the ethanol content of ethanol-water mixtures vaporizing from a LDO/fluoropolymer film.

	t_t	t_s	FWHM	dm/dt	$\Theta_{(t0)}$	$S_{w(ts)}$	$S_{d(t0)}$
A	891.19	810.88	314.25	−0.00052	18.72	0.1199	4.665E−09
B	−0.01671	−0.02453	−0.02270	0.04769	−0.03023	0.04910	0.20150
C	−103.053	−56.674	6.268	−0.00655	110.136	1.733	4.771
R^2	0.998	0.999	0.987	0.999	0.979	0.993	0.991

time-dependent evaporation of ethanol-water mixtures was studied by high speed camera (for contact angle measurements), infrared camera (for thermal imaging) and weight loss measurement. For the systematic evaluation of the droplet's evaporation rate, the surface tension of the ethanol/water mixture was tuned by the ratio of these two miscible solvents.

The evaporation of a liquid from LDO/fluoropolymer layer could be divided into three stages: in the I stage the dominant process is the evaporation of the sessile droplet with θ >90°; in the II stage the dominant process is the evaporation of the sessile droplet with θ <90° (until t_s) and in the III stage the dominant process is the evaporation of the liquid from the porous system (until t_t). Based on the results of the appropriate model calculation of the evaporation rate, we concluded that i) the evaporation rate for the divided stages of the vaporization is constant with a good approximation, ii) the evaporation rate decreases systematically in the successive stages, and iii) the evaporation rate increases with the increasing ethanol content examining a selected stage.

The wetting of the LDO/fluoropolymer layer increased with the increasing initial ethanol content of the applied liquid mixture. The Cassie's wetting mode was assigned to the pure water and the Wenzel's wetting mode to the ethanol, respectively. The surface free energy of the studied LDO/fluoropolymer composite was 8.4 ± 2.6 mN/m as determined by dynamic contact angle measurements and the heat transfer coefficient between the LDO/fluoropolymer layer and the water droplet was $K_T = 1768$ W/(m^{2}K) calculated from the appropriate evaporation rate model.

Under the applied experimental conditions, the LDO/fluoropolymer layer was completely stable at room temperature. However, the coffee ring effect could be observed at the end of the evaporation of pure ethanol at 50 °C, indicating a slight instability of the prepared layer. This instability is one limitation of the future application. The primary measurement methods (weight, temperature, contact angle) were not disturbed by the fact that the constitution of the evaporating liquid mixtures changes during the experiment, however, the continuous change of the liquid phase's constitution complicates the modelling of the evaporation process. Furthermore, this is a limitation of the future analytical application, because this method could be appropriate only to provide information on the initial composition of the liquids mixtures. Several experimentally determined parameters were used to characterize the evaporations of the different solvent mixtures. It was proven by using an appropriate statistical method, that these values are specific for the solvents, and can be used for both quantitative and qualitative analysis. Within the limits mentioned above, these results allow us to predict the possibility of using a similar setup in a potential future analytical chemistry application.

Table 5
Pearson correlation coefficient (PCC) matrix for the specific evaporation parameters from a LDO/fluoropolymer layer indicating total evaporation time: t_t, full width at half maximum: FWHM, evaporation rate: dm/dt, time of evaporation from the surface: t_s, initial area of the droplet: $S_{d(t0)}$, wetted area at t_s: $S_{w(ts)}$, initial contact angle ($\Theta_{(t0)}$), density: ρ, surface tension: γ, melting point: $T_{melting}$, boiling point: $T_{boiling}$, viscosity: η, dipole moment: p, molecular mass: M. The temperature of the solid was set to 50 °C. The droplets were 5 μL. (Highlighted in green: moderate correlation, in light blue: high correlation, in dark blue: very high correlation.)

	ρ	γ	$T_{melting}$	$T_{boiling}$	η	p	M
t_t[1]	0.95	0.95	0.91	0.96	-0.98	0.98	-0.90
FWHM[2]	0.93	0.97	0.89	0.94	-0.96	0.96	-0.88
dm/dt	0.92	0.58	0.97	0.89	-0.88	0.88	-0.97
t_s	0.92	0.97	0.87	0.93	-0.95	0.95	-0.86
$S_{d\ (t0)}$	-0.80	-0.47	-0.88	-0.75	0.75	-0.75	0.88
$S_{w\ (ts)}$	-0.92	-0.61	-0.97	-0.89	0.88	-0.88	0.97
$\Theta_{(t0)}$	0.94	0.96	0.90	0.95	-0.97	0.97	-0.89

[a]Average value.
[b]From mass measurements.

CRediT authorship contribution statement

Ildikó Y. Tóth: Investigation, Formal analysis, Visualization, Conceptualization, Writing - original draft, Writing - review & editing. **László Janovák:** Investigation, Formal analysis, Visualization, Writing - review & editing. **Erzsébet S. Bogya:** Conceptualization. **Ágota Deák:** Investigation, Formal analysis. **Imre Dékány:** Supervision, Funding acquisition. **Amit Rawal:** Conceptualization, Funding acquisition. **Ákos Kukovecz:** Conceptualization, Funding acquisition, Writing - review & editing.

Declaration of competing interest

The authors declare that they have no known competing financial interests or personal relationships that could have appeared to influence the work reported in this paper.

Acknowledgement

Financial support from the Hungarian Research, Development and Innovation Office (Hungary) through projects GINOP-2.3.2-15-2016-00013, K112531, and 2017-2.3.7-TÉT-IN-2017-00008, as well as from the Department of Science and Technology, Indian Ministry of Science and Technology through project 2017-2.3.7-STAKE-IN-2017-00008 (A.R.) is acknowledged. L. Janovák and E.S. Bogya were supported by the UNKP-18-4 New National Excellence and the NTP-NFTÖ-16 Programs of the Ministry of Human Capacities, respectively. I.Y. Tóth gratefully acknowledges the financial support of János Bolyai Research Fellowship of the Hungarian Academy of Sciences. The Ministry of Human Capacities, Hungary grant 20391-3/2018/FEKUSTRAT is also acknowledged.

Appendix A. Supplementary data

Supplementary data to this article can be found online at https://doi.org/10.1016/j.molliq.2020.112826.

References

[1] S.K. Singh, S. Khandekar, D. Pratap, S.A. Ramakrishna, Wetting dynamics and evaporation of sessile droplets on nano-porous alumina surfaces, Colloids Surf. A Physicochem. Eng. Asp. 432 (2013) 71–81, https://doi.org/10.1016/j.colsurfa.2013.04.070.

[2] D. Bonn, J. Eggers, J. Indekeu, J. Meunier, E. Rolley, Wetting and spreading, Rev. Mod. Phys. 81 (2) (2009) 739–804, https://doi.org/10.1103/RevModPhys.81.739.

[3] H.Y. Erbil, Evaporation of pure liquid sessile and spherical suspended drops: a review, Adv. Colloid Interf. Sci. 170 (1–2) (2012) 67–86, https://doi.org/10.1016/j.cis.2011.12.006.

[4] S.Y. Misyura, P.A. Strizhak, R.S. Volkov, V.S. Morozov, The influence of the wall microtexture on functional properties and heat transfer, J. Mol. Liq. 294 (2019), 111670. https://doi.org/10.1016/j.molliq.2019.111670.

[5] P. Tabeling, Foreword, Comptes Rendus Physique 5 (5) (2004) 519–520, https://doi.org/10.1016/j.crhy.2004.04.001.

[6] M. Abuku, H. Janssen, J. Poesen, S. Roels, Impact, absorption and evaporation of raindrops on building facades, Build. Sci. 44 (1) (2009) 113–124, https://doi.org/10.1016/j.buildenv.2008.02.001.

[7] A.G. Marin, H. Gelderblom, D. Lohse, J.H. Snoeijer, Order-to-disorder transition in ring-shaped colloidal stains, Phys. Rev. Lett. 107 (8) (2011), 085502. https://doi.org/10.1103/PhysRevLett.107.085502.

[8] S. Zhang, Q. Li, I.A. Kinloch, A.H. Windle, Ordering in a droplet of an aqueous suspension of single-wall carbon nanotubes on a solid substrate, Langmuir 26 (3) (2010) 2107–2112, https://doi.org/10.1021/la902642f.

[9] J. He, Q. Zhang, S. Gupta, T. Emrick, T.R. Russell, P. Thiyagarajan, Drying droplets: a window into the behavior of nanorods at interfaces, Small 3 (7) (2007) 1214–1217, https://doi.org/10.1002/smll.200700055.

[10] X. Fang, B. Li, E. Petersen, Y.-S. Seo, V.A. Samuilov, Y. Chen, J.C. Sokolov, C.Y. Shew, M.H. Rafailovich, Drying of DNA droplets, Langmuir 22 (14) (2006) 6308–6312, https://doi.org/10.1021/la060479u.

[11] N.J. Carroll, S.B. Rathod, E. Derbins, S. Mendez, D.A. Weitz, D.N. Petsev, Droplet-based microfluidics for emulsion and solvent evaporation synthesis of monodisperse mesoporous silica microspheres, Langmuir 24 (3) (2008) 658–661, https://doi.org/10.1021/la7032516.

[12] S.T. Chang, O.D. Velev, Evaporation-induced particle microseparations inside droplets floating on a chip, Langmuir 22 (4) (2006) 1459–1468, https://doi.org/10.1021/la052695t.

[13] M. Singh, H.M. Haverinen, P. Dhagat, G.E. Jabbour, Inkjet printing-process and its applications, Adv. Mater. 22 (6) (2010) 673–685, https://doi.org/10.1002/adma.200901141.

[14] R. Picknett, R. Bexon, The evaporation of sessile or pendant drops in still air, J. Colloid Interface Sci. 61 (1977) 336–350, https://doi.org/10.1016/0021-9797(77)90396-4.

[15] S.A. Kulinich, M. Farzaneh, Effect of contact angle hysteresis on water droplet evaporation from super-hydrophobic surfaces, Appl. Surf. Sci. 255 (7) (2009) 4056–4060, https://doi.org/10.1016/j.apsusc.2008.10.109.

[16] A. Rawal, Design parameters for a robust superhydrophobic electrospun nonwoven mat, Langmuir 28 (6) (2012) 3285–3289, https://doi.org/10.1021/la204535s.

[17] G. McHale, S. Aqil, N.J. Shirtcliffe, M.I. Newton, H.Y. Erbil, Analysis of droplet evaporation on a superhydrophobic surface, Langmuir 21 (24) (2005) 11053–11060, https://doi.org/10.1021/la0518795.

[18] Z. Pan, S. Dash, J.A. Weibel, S.V. Garimella, Assessment of water droplet evaporation mechanisms on hydrophobic and superhydrophobic substrates, Langmuir 29 (51) (2013) 15831–15841, https://doi.org/10.1021/la4045286.

[19] R.-H. Chen, T.X. Phuoc, D. Martello, Effects of nanoparticles on nanofluid droplet evaporation, Int. J. Heat Mass Transf. 53 (19–20) (2010) 3677–3682, https://doi.org/10.1016/j.ijheatmasstransfer.2010.04.006.

[20] R. Bhardwaj, An Investigation of the Evaporation of a Droplet on a Solid Surface: Evaporation, Self-assembly of Colloidal Deposits, and Interfacial Heat Transfer, (PhD. thesis) Columbia University, 2010.

[21] R.D. Deegan, O. Bakajin, T.F. Dupont, G. Huber, S.R. Nagel, T.A. Witten, Capillary flow as the cause of ring stains from dried liquid drops, Nature 389 (6653) (1997) 827–829, https://doi.org/10.1038/39827.

[22] H.Z. Wang, Z.P. Huang, Q.J. Cai, K. Kulkarni, C.-L. Chen, D. Carnahan, Z.F. Ren, Reversible transformation of hydrophobicity and hydrophilicity of aligned carbon nanotube arrays and buckypapers by dry processes, Carbon 48 (3) (2010) 868–875, https://doi.org/10.1016/j.carbon.2009.10.041.

[23] F. Trifiro, A. Vaccari, Hydrotalcite-like anionic clays (layered double hydroxides), in: J.L. Atwood, J.E.D. Davies, D.D. Macnicol, F. Vögtle, J.M. Lehn (Eds.), Comprehensive Supramolecular Chemistry, vol. 7, Pergamon, Oxford 1996, pp. 251–290.

[24] E. Geraud, V. Prevot, F. Leroux, Synthesis and characterization of macroporous MgAl LDH using polystyrene spheres as template, J. Phys. Chem. Solids 67 (5–6) (2006) 903–908, https://doi.org/10.1016/j.jpcs.2006.01.002.

[25] P. Sipos, I. Palinko, As-prepared and intercalated layered double hydroxides of the hydrocalumite type as efficient catalysts in various reactions, Catal. Today 36 (2018) 147, https://doi.org/10.1016/j.cattod.2016.12.004.

[26] W. Wang, J. Zhou, G. Achari, J. Yu, W. Cai, Cr(VI) removal from aqueous solutions by hydrothermal synthetic layered double hydroxides: adsorption performance, coexisting anions and regeneration studies, Colloids Surf. A Physicochem. Eng. Asp. 457 (2014) 33–40, https://doi.org/10.1016/j.colsurfa.2014.05.034.

[27] Y. Wu, Y. Yu, J.Z. Zhou, J. Liu, Y. Chi, Z.P. Xu, G. Qian, Effective removal of pyrophosphate by CaFe-LDH and its mechanism, Chem. Eng. J. 179 (2012) 72–79, https://doi.org/10.1016/j.cej.2011.10.053.

[28] Y. Li, S. Li, Y. Zhang, M. Yu, J. Liu, Fabrication of superhydrophobic layered double hydroxides films with different metal cations on anodized aluminum 2198 alloy, Mater. Lett. 142 (2015) 137–140, https://doi.org/10.1016/j.matlet.2014.11.148.

[29] K. Shanmuganathan, C.J. Ellison, Layered double hydroxides: an emerging class of flame retardants, Polym. Green Flame Retardants 20 (2014) 675–707, https://doi.org/10.1016/B978-0-444-53808-6.00020-2.

[30] C.D. Hoyo, Layered double hydroxides and human health: an overview, Appl. Clay Sci. 36 (2007) 103–121, https://doi.org/10.1016/j.clay.2006.06.010.

[31] L. Mohapatra, K. Parida, A review on the recent progress, challenges and perspective of layered double hydroxides as promising photocatalysts, J. Mater. Chem. A 4 (2016) 10744–10766, https://doi.org/10.1039/C6TA01668E.

[32] Á. Deák, L. Janovák, E. Csapó, D. Ungor, I. Pálinkó, S. Puskás, T. Ördög, T. Ricza, I. Dékány, Layered double oxide (LDO) particle containing photoreactive hybrid layers with tunable superhydrophobic and photocatalytic properties, Appl. Surf. Sci. 389 (2016) 294–302, https://doi.org/10.1016/j.apsusc.2016.07.127.

[33] N. Shokri, M. Sahimi, D. Or, Morphology, propagation dynamics and scaling characteristics of drying fronts in porous media, Geophys. Res. Lett. 39 (2012), L09401. https://doi.org/10.1029/2012GL051506.

[34] R. Wu, G.-M. Cui, R. Chen, Pore network study of slow evaporation in hydrophobic porous media, Int. J. Heat Mass Transf. 68 (2014) 310–323, https://doi.org/10.1016/j.ijheatmasstransfer.2013.09.042.

[35] K. Sefiane, M.E.R. Shanahan, M. Antoni, Wetting and phase change: opportunities and challenges, Curr. Opin. Colloid Interface Sci. 16 (2011) 317–325, https://doi.org/10.1016/j.cocis.2011.03.003.

[36] K. Sefiane, R. Bennacer, Nanofluids droplets evaporation kinetics and wetting dynamics on rough heated substrates, Adv. Colloid Interf. Sci. 147-148 (2009) 263–271, https://doi.org/10.1016/j.cis.2008.09.011.

[37] S.Y. Misyura, Contact angle and droplet heat transfer during evaporation on structured and smooth surfaces of heated wall, Appl. Surf. Sci. 414 (2017) 188–196, https://doi.org/10.1016/j.apsusc.2017.03.288.

[38] S. David, K. Sefiane, L. Tadrist, Experimental investigation of the effect of thermal properties of the substrate in the wetting and evaporation of sessile drops, Colloids Surf. A Physicochem. Eng. Asp. 298 (2007) 108–114, https://doi.org/10.1016/j.colsurfa.2006.12.018.

[39] G. Schuszter, E.S. Bogya, D. Horváth, Á. Tóth, H. Haspel, Á. Kukovecz, Liquid droplet evaporation from buckypaper: on the fundamental properties of the evaporation profile, Microporous Mesoporous Mater. 209 (2015) 105–112, https://doi.org/10.1016/j.micromeso.2015.02.025.

[40] E. Nefzaoui, O. Skurtys, Impact of a liquid drop on a granular medium: inertia, viscosity and surface tension effects on the drop deformation, Exp. Thermal Fluid Sci. 41 (2012) 43–50, https://doi.org/10.1016/j.expthermflusci.2012.03.007.

[41] E.S. Bogya, B. Szilagyi, Á. Kukovecz, Surface pinning explains the low heat transfer coefficient between water and a carbon nanotube film, Carbon 100 (2016) 27–35, https://doi.org/10.1016/j.carbon.2015.12.077.

[42] A. Deak, L. Janovak, S.P. Tallosy, T. Bito, D. Sebok, N. Buzas, I. Palinko, I. Dekany, Spherical LDH-Ag degrees -montmorillonite heterocoagulated system with a pH-dependent sol-gel structure for controlled accessibility of AgNPs immobilized on the clay lamellae, Langmuir 31 (6) (2015) 2019–2027, https://doi.org/10.1021/la504096t.

[43] L. Janovák, S.P. Tallósy, M. Sztakó, Á. Deák, T. Bitó, N. Buzás, G. Bártfai, I. Dékány, Synthesis of pH-sensitive copolymer thin solid films embedded with silver nanoparticles for controlled release and their fungicide properties, J. Drug Delivery Sci. Technol. 24 (6) (2014) 628–636, https://doi.org/10.1016/S1773-2247(14)50129-3.

[44] E. Chibowski, Surface free energy of a solid from contact angle hysteresis, Adv. Colloid Interf. Sci. 103 (2003) 149–172, https://doi.org/10.1016/S0001-8686(02)00093-3.

[45] V.M. Starov, S.R. Kostvintsev, V.D. Sobolev, M.G. Velarde, S.A. Zhdanov, Spreading of liquid drops over dry porous layers: complete wetting case, J. Colloid Interface Sci. 252 (2002) 397–408, https://doi.org/10.1006/jcis.2002.8450.

[46] V.M. Starov, S.A. Zhdanov, S.R. Kosvintsev, V.D. Sobolev, M.G. Velarde, Spreading of liquid drops over porous substrates, Adv. Colloid Interf. Sci. 104 (2003) 123–158, https://doi.org/10.1016/S0001-8686(03)00039-3.

[47] V.M. Starov, S.R. Kosvintsev, V.D. Sobolev, M.G. Velarde, S.A. Zhdanov, Spreading of liquid drops over saturated porous layers, J. Colloid Interface Sci. 246 (2002) 372–379, https://doi.org/10.1006/jcis.2001.8077.

[48] P. Kavehpour, B. Ovryn, G.H. McKinley, Evaporatively-driven Marangoni instabilities of volatile liquid films spreading on thermally conductive substrates, Colloids Surf. A Physicochem. Eng. Asp. 206 (2002) 409–423, https://doi.org/10.1016/S0927-7757(02)00064-X.

[49] M. Reyssat, J.M. Yeomans, D. Quéré, Impalement of fakir drops, EPL 81 (2) (2008), 26006. https://doi.org/10.1209/0295-5075/81/26006.

[50] K.S. Birdi, D.T. Vu, Wettability and the evaporation rates of fluids from solid-surfaces, J. Adhes. Sci. Technol. 7 (6) (1993) 485–493, https://doi.org/10.1163/156856193X00808.

[51] G. McHale, S.M. Rowan, M.I. Newton, M.K. Banerjee, Evaporation and the wetting of a low-energy solid surface, J. Phys. Chem. B 102 (11) (1998) 1964–1967, https://doi.org/10.1021/jp972552i.

[52] H. Hu, R.G. Larson, Evaporation of a sessile droplet on a substrate, J. Phys. Chem. B 106 (2002) 1334–1344, https://doi.org/10.1021/jp0118322.

[53] R.D. Deegan, O. Bakajin, T.F. Dupont, G. Huber, S.R. Nagel, T.A. Witten, Contact line deposits in an evaporating drop, Phys. Rev. E 62 (2000) 756–765, https://doi.org/10.1103/PhysRevE.62.756.

[54] H.A. Duguid, A Study of the Evaporation Rates of Small Freely Falling Water Droplets Droplets, Masters Theses University of Missouri, Rolla, 1969.

[55] G. Rugg, Using Statistics: A Gentle Introduction, first ed. McGrow-Hill, Maidenhead, 2007.

[56] D.E. Hinkle, W. Wiersma, S.G. Jurs, Applied Statistics for the Behavioral Sciences, 5th ed. Houghton Mifflin, Boston, 2003.